Monitoring of Hydration Processes in Cement Materials by Broadband Time-Domain-Reflectometry Dielectric Spectroscopy

N.E. Hager III and R.C. Domszy
Material Sensing & Instrumentation, 772 Dorsea Rd. Lancaster PA 17601 USA
Dept. Physics and Engineering Elizabethtown College, Elizabethtown PA 17022 USA

Keywords: TDR, Cement, Hydration, Sensor

Abstract

Prior work in our laboratory demonstrated a continuous monitoring of the chemical state of water in hydrating cement paste, over the frequency range 10 kHz to 8 GHz and from initial mixing to several weeks cure. The broadband complex permittivity is obtained over the range using Time-Domain-Reflectometry (TDR) Dielectric Spectroscopy, using Fourier transform methods and an embedded capacitance sensor. Three fundamental signals are identified, corresponding to unreacted free water appearing near 10 GHz, bound-water attaching to developing microstructure near 100 MHz, and grain polarization occurring around 1 MHz. The three signal components are fit to appropriate molecular models as a function of cure time and monitored throughout the process. The result is 1) a free-water relaxation which monitors the disappearance of water into hydration and thus follows percent hydration, and 2) a bound-water relaxation which monitors water attaching to developing microstructure and thus monitors formation of this microstructure, and 3) a grain-polarization component which monitors developing microstructure.

Our current work focuses on investigating changes in this relaxation spectrum and its cure evolution with changes in chemistry and processing conditions. Using the full frequency transform, we explore relative changes in various signal components with changes in ionic strength and backfilling of the pore space with excess free water. Monitoring the transient amplitude directly, we follow specific frequency components by monitoring corresponding delay times and follow reaction rates in the time domain. Changes in reaction rate are compared for changes in temperature, addition of accelerants and retarders, and other factors. Reaction rates obtained by TDR are also compared with rates obtained by other measures of cement hydration; such as heat evolution by isothermal calorimetry, bound-water formation by thermogravimetric analysis, and calcium hydroxide production by differential scanning calorimetry. The transient analysis can be integrated with a small portable TDR sampler to form a robust cure-monitoring system usable in the field.

Introduction

The compressive strength of concrete and its loading capabilities are directly related to the ratio of water to cement solids (w/c) and degree of hydration in the cement paste, and to a lesser extent the size, shape, and strength of the aggregate used. The initial w/c ratio of the mix is the largest single factor influencing the strength of compacted concrete[1] and a continuous measure of w/c ratio during cement cure is known to be a predictor of concrete strength.[2,3,4] Concrete with lower water/cement ratio (down to 0.35) makes a stronger concrete than a higher ratio, and certain chemical additives such as water reducers strengthen concrete by allowing a flowable concrete with less water than without such additives. The ability to accurately quantify the water

to cement ratio and degree of hydration in the cement paste is an important benefit in characterizing strength and service life of concrete structures.

Our research explores a new method of monitoring hydration in cement and concrete materials[5]. The material is embedded with an inexpensive capacitance sensor and interrogated by broadband Time-Domain-Reflectometry (TDR) Dielectric Spectroscopy, providing a molecular rotation spectrum of water over an extremely wide frequency range. Three separate states of water participating in the hydration reaction are identified, including a free-water rotational state, a bound-water rotational state, and an ion-hopping state. The 3 states are fit to appropriate models as a function of cure time, and a variation in cement chemistry reveals the nature of the processes involved.

A unique aspect of the system is that the measurement is performed in the time domain, where sensor response is separated from instrument artifacts by propagation delay. Data can be either transformed to a microwave frequency spectrum for scientific-quality analysis, or interpreted directly in the time domain for robust field-grade control. This simplifies the measurement for field use, where the amplitude of the reflected transient can be followed directly without phase-sensitive frequency transform using inexpensive PC-based instruments.

Experimental

The expressions governing TDR Dielectric Spectroscopy are described in the literature.[6] The sample permittivity $\varepsilon^*(\omega)$ is related to the Laplace Transforms of the incident $v_o(\omega)$ and reflected $r(\omega)$ pulses according to:

$$\varepsilon^*(\omega) = \frac{G_c}{\iota\omega C_o}\frac{[v_o(\omega) - r(\omega)]}{[v_o(\omega) + r(\omega)]} \qquad (1)$$

where C_o is the geometric capacitance of the empty sensor, G_c the characteristic line admittance, and ω the frequency. Refinements including bilinear calibration and nonuniform sampling are described in the literature.[7]

The sensor is a 3.6 mm diameter semi-rigid coaxial line with a short section of inner conductor protruding at its tip (Figure 1). Since the exposed tip is an effective radiator in high-permittivity liquids, it is shielded with a serrated castle nut, which provides a surrounding ground plane while allowing free-flow of material through the tip.

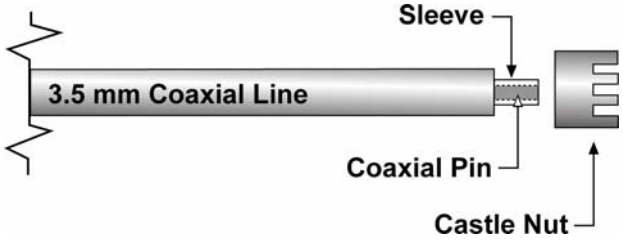

Figure 1 – Schematic of cement sensor.

A reference portland cement was obtained from the Cement and Concrete Reference Laboratory (CCRL) at NIST. The material is an ASTM Type I ordinary portland cement (reference number 135) with a Blaine fineness of 394 m^2/kg.[8,9] Starting powders are mixed with distilled water in a water-to-cement ratio of 0.4 by weight.

The sample is placed in a sealed container with the sensor line extending through a rubber septum in the lid. Samples are placed in a temperature-controlled water bath with thermocouples recording the temperature. Data is acquired every 10-15 minutes initially, then slowed after

several days cure. Acquisition is PC-automated, with all data records, calibration records, temperature, and timestamps stored in a common datafile for later analysis. A typical cure run records 3-400 individual records as a function of cure time, so monitoring is continuous.

Frequency Domain Results

Basic Signal Evolution

Figure 2 shows the real and imaginary permittivity during the cure of portland cement over the frequency range 10 kHz to 8 GHz. The initial real permittivity ε′ in Figure 2a shows a broad flat region above 10^7 Hz due to free-water response and a large increase below 10^7 Hz due to electrode polarization. During the cure process, the high-frequency permittivity near 10 GHz decreases as free water is consumed in the reaction, while an intermediate-frequency signal grows around 10 MHz indicating reaction products forming during the process.

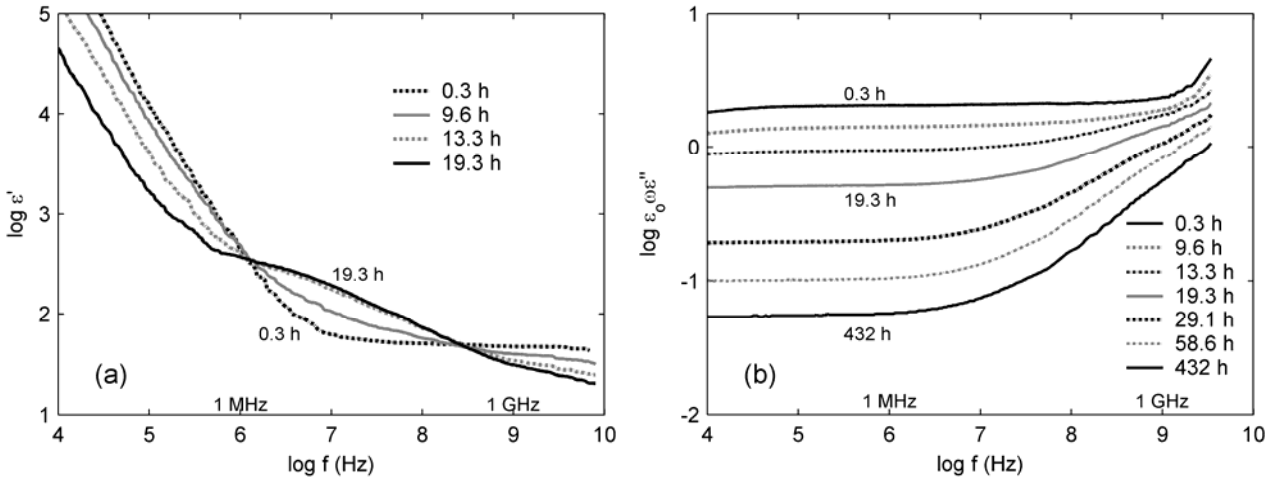

Figure 2 – Real and imaginary permittivity evolution during portland cement cure.

The imaginary permittivity is displayed as dielectric conductivity $\varepsilon_o\omega\varepsilon''$ to remove the ω^{-1} dependence and accentuate small differences above 1 MHz. The initial conductivity in Figure 2b shows a large flat baseline across the frequency range representing DC conductivity. As cure proceeds the conductivity decreases, as seen by the decreasing baseline, and an intermediate-frequency signal grows as a deviation from the baseline around 100 MHz indicating reaction products forming during the process.

The intermediate-frequency signals are not present in the initial cement paste but only appear after several hours cure, indicating some additional states forming with developing microstructure. Signals appearing in permittivity and conductivity show separate relaxation frequencies, and are not real and imaginary counterparts of one another. We thus have two intermediate-frequency signals, each with permittivity and conductivity components, which we designate the low and medium relaxations.

Modeling and Model Evolution

A typical model fit is shown in Figure 3, where a broad Cole-Davidson relaxation and two narrow Debye relaxations are fit across the entire frequency range. Both real and imaginary components are fit simultaneously using shared parameters, with the frequencies, amplitudes, and distribution factors extracted as a function of cure time. For the permittivity, the model replicates

the electrode polarization below 1 MHz, the low relaxation from 1 MHz to 1 GHz, and the free relaxation above 1 GHz. The fit is superimposed on the measured data along with individual model contributions. For the conductivity, the model replicates the conducting baseline below 10 MHz along with the upturn above 10 MHz due to the medium and free relaxations. The fit is again superimposed on the measured data along with individual contributions, and it is clear that the additional medium relaxation is required to replicate the conductivity behavior. Combinations of model components are subtracted from the actual signal and the residual signal examined, to be sure both low- and medium-relaxations are present with both real and imaginary components.

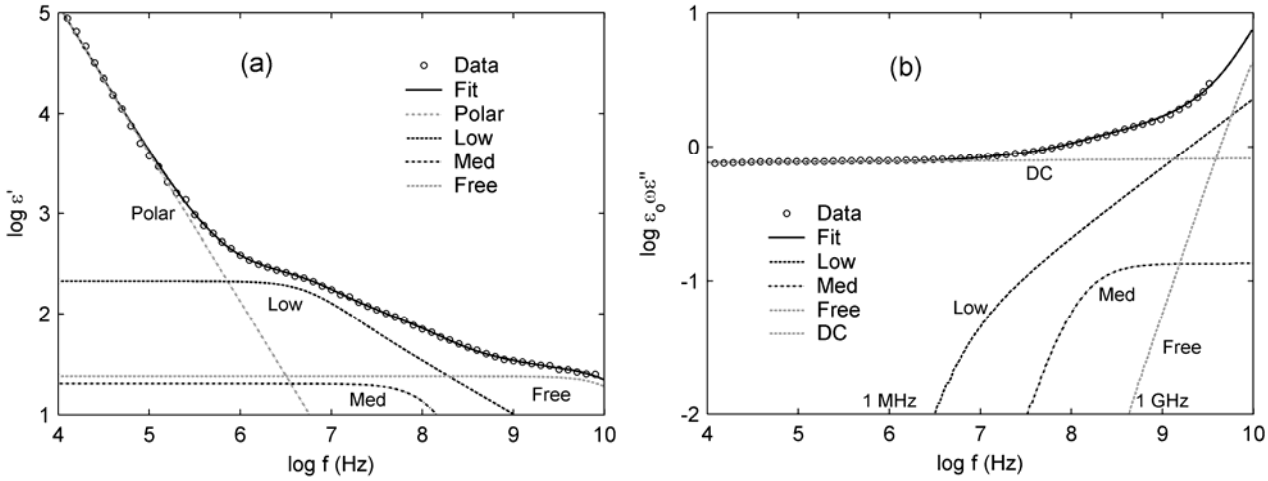

Figure 3 - Model fitting to real and imaginary permittivity at 15 h cure.

The model evolution is now monitored continuously during the cure process by fitting the model continuously as a function of cure time. The free-relaxation amplitude begins around 40, corresponding to the volume reduction of water to cement in the initial cement paste. The amplitude decreases with cure time, showing a rapid decrease during the first 20 hours and a more gradual decrease thereafter. The low-relaxation amplitude begins at zero and rises to an effective permittivity near 300 at 20 hours. It then decreases slowly with cure time for all times thereafter. The medium-relaxation amplitude begins at zero, and rises to a permittivity near 30 at 20 hours and decreases for all times thereafter. The conductivity amplitude decreases from 2 S/m to 0.1 S/m during the period, in accordance with low frequency results.

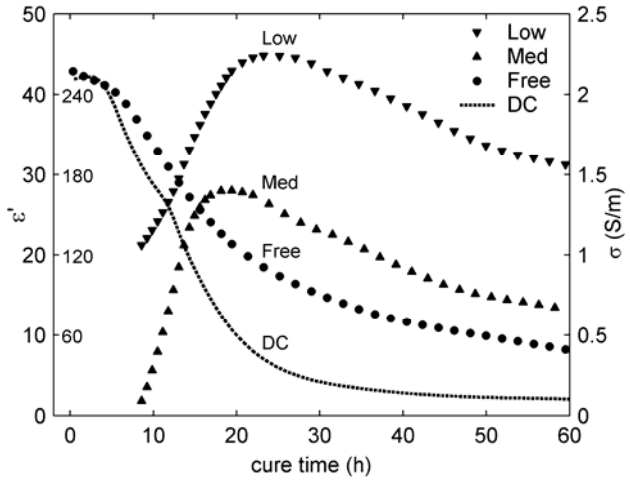

Figure 4 – Evolution of model components during 60 h cure.

Material Variations

Variation in Ion Content

The low relaxation is significantly affected by a varying ion content[5], either by substituting tricalcium silicate as the hydrating paste or by comparing tricalcium silicate with varying ion content. This is seen in Figure 5a, where a tricalcium silicate sample is hydrated with and without potassium sulfate. The low-relaxation amplitude increases with increasing ion concentration yet retains a relaxation distinct from DC conductivity. We attribute this to a grain-polarization model[10,11] in which double layer processes operating on the gel surface increase the polarizability at frequencies just above electrode polarization. The medium relaxation on the other hand, is relatively unchanged and we attribute this to bound-water model[3] in which water binds to developing microstructure and takes on a relaxation distinct from pure water. Similar behavior is seen in a variety of organic/inorganic systems.[12,13,14]

Variation in Excess Pore Water

The free-water and ion conductivity contributions are significantly affected by addition of excess pore water while the low relaxation remains relatively constant. This is seen in Figure 5b where a 50 mm mortar cube with a sensor at its center is submerged in water at 24 h cure. Both the free-water permittivity near 10 GHz and the electrode polarization below 100 kHz increase over a period of 6 hours, as the sample remains submerged and water fills the pore space. The increased electrode polarization reflects an increased conductivity in the sample, which is seen in the imaginary counterpart to Figure 5b. Pore water variation thus shows the opposite of ionic strength variation, as the free water and electrode polarization increase while the low relaxation remains relatively constant.

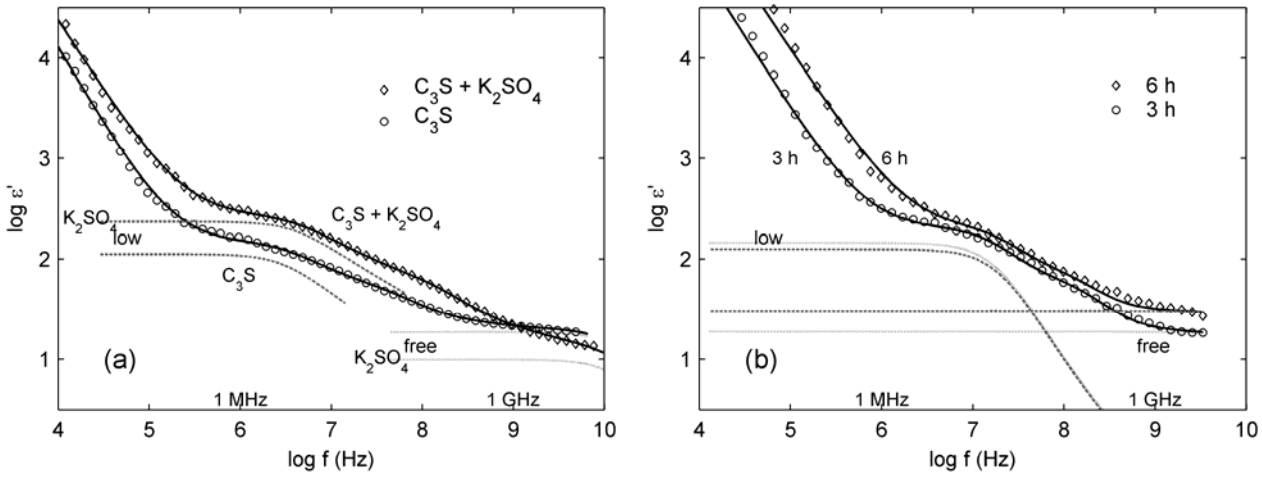

Figure 5 - Effect of ionic strength and excess pore water at ~24 h cure.

Time Domain Analysis and Applications

TDR offers an advantage over frequency-domain methods in the rate-dependent information can be interpreted directly in the time domain. From Fourier analysis, the 10 GHz response is concentrated near the peak of the reflected transient in the picosecond range, while ~100 MHz and ~1 MHz response is concentrated at later times in the transient in the nanosecond/ microsecond ranges. By monitoring the amplitude near the transient peak we monitor the 10 GHz

permittivity indirectly, and thus follow only the free-water concentration since all other effects including bound water and ion conductivity cannot respond at these frequencies.

Separation of Fast Polar Response from Conductivity

An example is shown in Figure 6. A sensor is inserted in a test fluid and interrogated with a 35 ps pulse, with the response displayed on a logarithmic time scale. The transient is inverted in the usual manner, showing the empty-sensor reflection at the top and increasing sensor loading toward the bottom. In Figure 6a the test fluid is varied among dielectric reference liquids of increasing permittivity, from dichloromethane (ε' = 8.9), to acetone (ε' = 21.1), to acetonitrile (ε' = 37.5), to deionized water (ε' = 78). The reflected signal shows an increasing amplitude with each liquid on the 100 ps time scale, since each liquid has a fast dipole rotation which can respond at these speeds. In Figure 6b the deionized water is measured again, but now with increasing amounts of salt concentration. The initial increase at short times remains unchanged, but now an additional loading is seen on longer time scales due to slow-responding conducting ions. The short-time permittivity is dependent on material and independent of conductivity, so the measurement is chemical-specific.

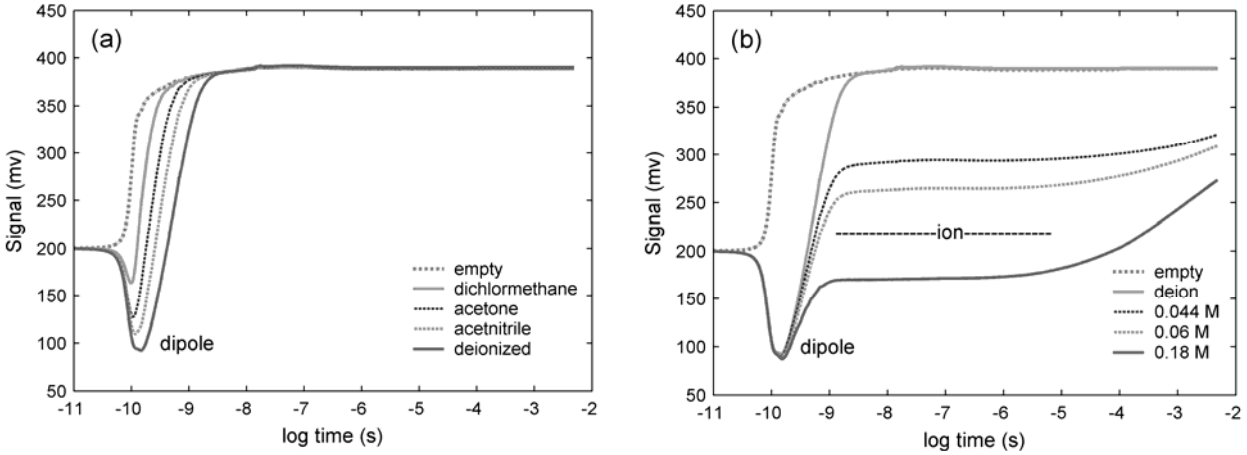

Figure 6 – TDR reflection for (a) varying permittivity (b) varying conductivity.

Separation of Portland Cement Components

Figure 7 shows the direct transient for portland cement from which Figure 2 is derived. The signal is captured on 7 successive time scales, beginning at 20 ps/cm on the left and ending at 500 μs/cm on the right. The transient is displayed on a piecewise-linear scale where multiple relaxations at intermediate times are more easily seen. Constant-permittivity reference liquids acetone (ε′ = 21.1) and acetonitrile (ε′ = 37.5) are shown showing the exponential decay of a constant sensor capacitance in series with the 50-ohm line. Also shown is the cement paste, which shows a superexponential decay spanning many decades due to the frequency-dependent sample permittivity. At 1 hour the transient shows a large amplitude on the 20 ps/cm timescale, indicating free-water activity, followed by a long baseline on later timescales indicating ion conduction. At 20 hours the transient shows a smaller amplitude on 20 ps/cm timescale, indicating reduced free-water activity, followed by a continuing decay on later timescales indicating additional relaxations. The conducting baseline decreases with decreasing ion conductivity.

A simple indicator for the free relaxation is the amplitude on the 20 ps/cm scale near the peak of the reflected signal. The delay time is approximately 100 ps, representing response in the gigahertz frequency range ($\omega = 1/t$). A simple indicator for the low relaxation is the amplitude on the 500 ps scale, where the reference transients have decayed to zero yet continuing cement decay is seen. The delay here is around 1 ns, representing response in the sub-gigahertz frequency range. To remove conductivity the baseline at 100 ns is subtracted, leaving a difference signal above the conductivity which cannot be accounted for by free-water relaxation.

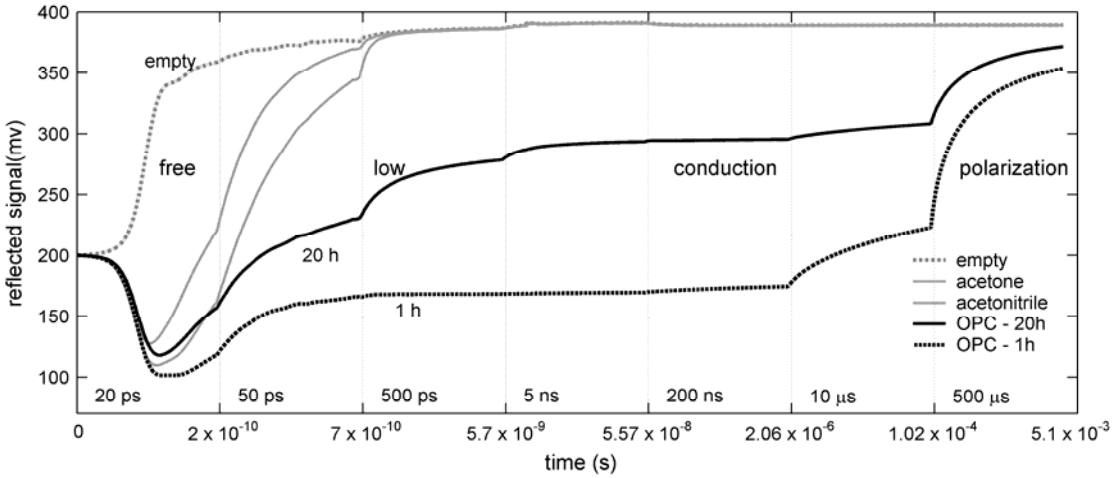

Figure 7 - TDR reflected transient over 7 times scales during cement hydration.

Since the free-relaxation indicator scales with free-water concentration, and the low-relaxation indictor scales with microstructure formation, we can use these simple indicators to study variations in reaction rate between different cement formulations and cure conditions. An example is shown in Figure 8, where both the free-relaxation indicator and low relaxation indicator are followed as a function of cure time for variations in process conditions. As expected the free-relaxation indicator decreases with cure time while the low relaxation indicator increases to around 20 hours, and then decrease for all times thereafter.

Variation in Material and Processing Conditions

Our long-term focus is to compare the evolution of various signal components, in either time or frequency domain, with expected chemical and material changes through a combination of analytical measurement, chemical variation, and experimental investigation. Some areas include 1) correlating the disappearance of free water near 10 GHz with the increase in hydration through differential scanning calorimetry and thermogravimetric analysis, 2) correlating the increase in bound water near 100 MHz with the formation of reaction products as determined by quasi-elastic neutron scattering (QENS), optical microscopy, and other methods, 3) estimating the free-water loss to evaporation by instrumenting a large test cylinder with sensors at varying depths to determine moisture gradients, 4) examining variations in cement chemistry and their effect on signal evolution, and 5) exploring the thermodynamics of the relaxation processes with respect to pore size by freezing the material during hydration.

Some immediate variations considered here include effects of 1) temperature, 2) addition of chemical retarders, 3) comparison of free-water evolution with exothermic heat of reaction by isothermal calorimetry, 4) comparison of free-water evolution with non-evaporable water content by thermogravimetric analysis, 5) comparison of free-water evolution with calcium hydroxide

production by differential scanning calorimetry, 6) monitoring of excess pore water, and 7) monitoring of hydration in precast-grade concrete.

Variation in Temperature

The free- and low-relaxation indicators show the variation in hydration rate with changing cure temperature. Figure 8a shows the evolution of both indicators for two portland cement pastes undergoing cure at different temperatures. One sample is at 23.0 ± 0.5°C and the other at 30.0 ± 0.5°C. The 30°C sample shows a faster decay of the free-relaxation indicator, as well as a faster growth of the low-relaxation indicator and an earlier signal maximum. All other changes are roughly the same in both cases.

Addition of Retarders

The free- and low-relaxation indicators also show a decrease in hydration rate with the addition of chemical retarders. Figure 8bshows the evolution of both indicators for two portland cement pastes undergoing cure under identical conditions, with one sample prepared neat and the other containing 288 ppm sodium gluconate retarder. The retarder sample shows a slower decay of the free-relaxation indicator, as well as a slower growth of the low-relaxation indicator and a later signal maximum. Both samples are prepared using CCRL 135 portland cement in a w/c ratio of 0.42, with both containing F-35 sand in a ratio of 1:1 and cured at 22°C.

Comparison with Heat of Reaction

The free-relaxation indicator can be correlated with the exothermic heat of reaction as measured by isothermal calorimetry. The results are shown in Figure 8a where the heat of hydration determined from calorimetry is normalized by the published volumetric phase compositions of portland cement and the known values of the heat of hydration of the major phases in cement.[15] It is clear that the 100 ps transient amplitude follows a similar evolution with cure time, with the amplitude scaling and offset adjusted for convenience.

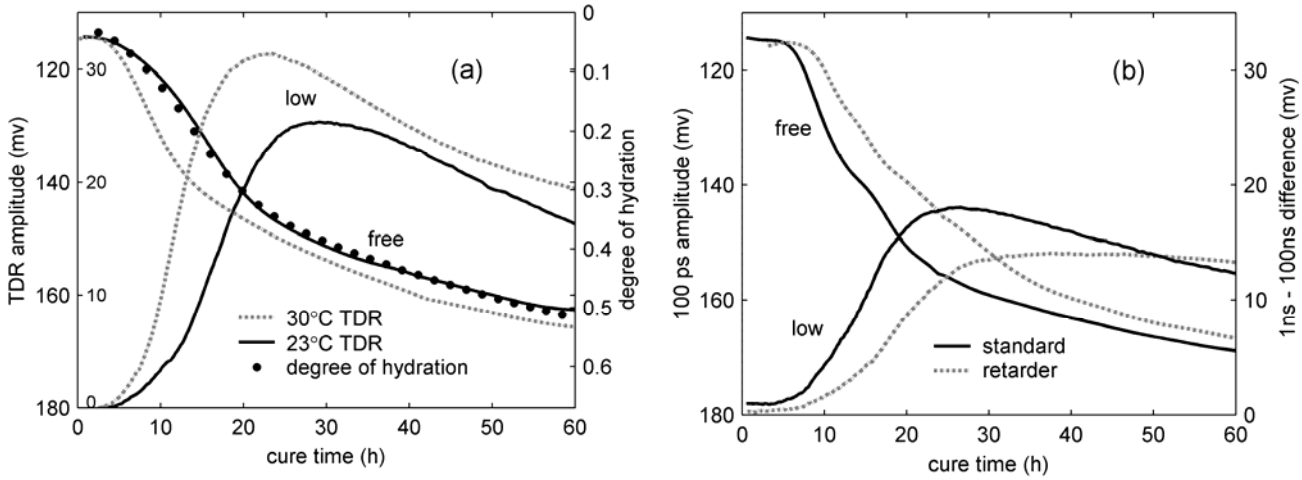

Figure 8 – Temperature variation and addition of retarders.

Comparison with Non-Evaporable Water Content

The free-relaxation indicator can be compared with degree of hydration as measured by thermogravimetric analysis, since the measured signal corresponds to the volume fraction of unreacted water in the cement paste which is the inverse of the degree of hydration. A sample is

embedded with both a TDR sensor and thermocouple probe and monitored continuously as a function of cure time. Side-samples of the material are tested by thermogravimetric analysis at regular intervals, revealing the amount of evaporable and non-evaporable water content. The free-relaxation amplitude is proportional to the volume fraction of water in the cement paste, so its decrease during cure follows a simultaneous increase in percent hydration as determined from non-evaporable water content. Results are shown in Figure 9a

Comparison with CaOH Production

The free-relaxation indicator can be compared with the concentration of calcium hydroxide as measured by Differential Scanning Calorimetry (DSC), since the disappearance of unreacted free water should correspond with the appearance of calcium hydroxide by reaction. For each measurement 12 side-samples are extracted to sealed centrifuge tubes, and stored in the bath along with the TDR sample. Samples are opened at regular intervals and a Perkin-Elmer DSC System 4 used to determine the calcium hydroxide content. Hydration was blocked in individual samples at specified times by grinding in the presence of acetone, filtering on a 0.7 micron glass filter, rinsing the residue and transferring to a vacuum oven at 40°C, and drying for 2 hours. Figure 9b shows the TDR amplitude plotted in solid lines and the DSC endotherm plotted in symbols, with the vertical scaling and offset between axes adjusted for best fit.

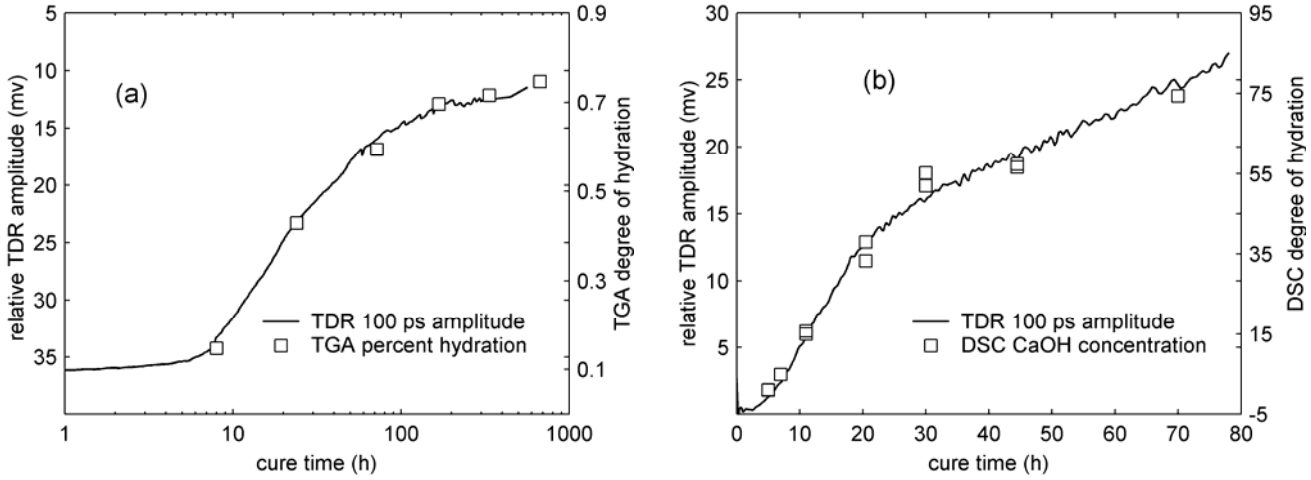

Figure 9 (a) Comparison of TDR unreacted water with TGA non-evaporable water content. (b) Comparison of TDR unreacted water with CaOH concentration.

Monitoring of Excess Pore Water

The free-relaxation indicator can be used to monitor the backfilling of pore water into a cured 50 mm mortar cube with a sensor embedded in its center. Figure 10a shows the 100 ps amplitude as a function of time after the dry cube is submerged in a water bath. The signal is stable for around 30 hours, then begins to increase on the inverted axis as water fills the pore space, and then at longer times begins to level off. A similar plot at 1 μs delay, where ion conduction dominates, shows a completely different signal evolution.

Monitoring of Precast Concrete Hydration

The free-relaxation indicator can be used to monitor hydration in production-grade concrete. A bucket is obtained from a local precast plant and returned immediately to the lab with a sensor and thermocouple probe inserted. The Fourier-transform spectrum is verified, showing

the same free, bound, and grain-polarization components as in cement paste, though with a reduced amplitude due to the lower water/solids ratio. Figure 10b shows the free-water indicator for 2 different batch runs along with the reaction exotherm, and it is clear that the maximum rate of disappearance of free water corresponds to the maximum reaction exotherm.

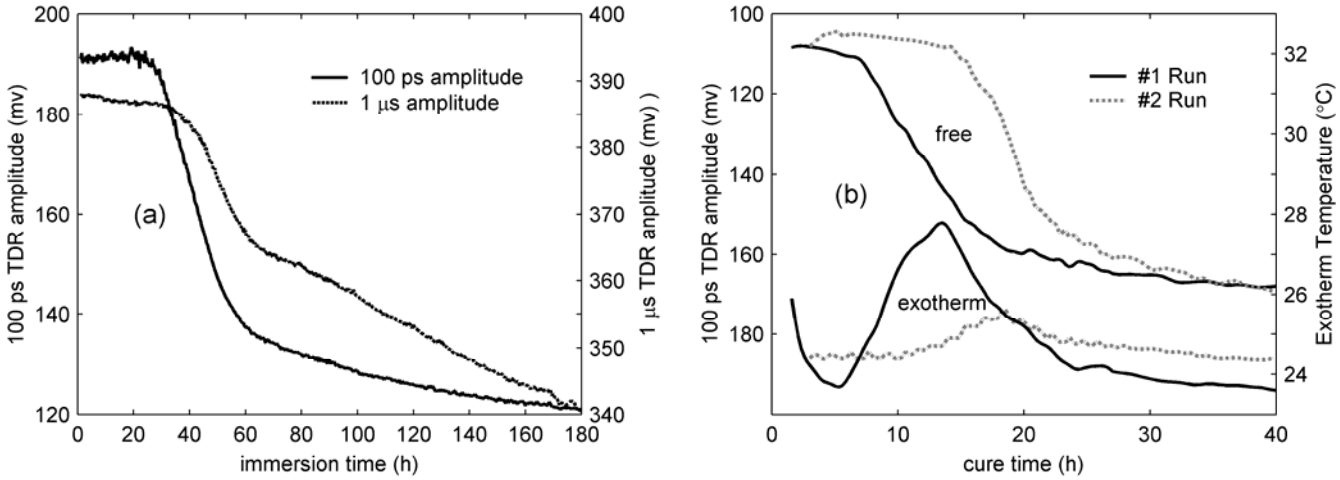

Figure 10 (a) Monitoring of excess pore water during backfilling of pore water. (b) Monitoring of hydration in precast concrete and reaction exotherm.

Conclusions

Time-Domain-Reflectometry Dielectric Spectroscopy provides a continuous monitor of the chemical state of water in hydrating cement materials over the frequency range 10 kHz to 10 GHz and from initial mixing to long-time cure. Three fundamental signals are identified, corresponding to unreacted free water appearing near 10 GHz, bound-water attaching to developing microstructure near 100 MHz, and grain polarization occurring around 1 MHz. The three signal components are fit to appropriate molecular models as a function of cure time and monitored throughout the process.

We can use this behavior to explore variations in cement chemistry and processing conditions. Using the full frequency transform, we show an increase in grain polarization with increases in ionic strength, and an increase in free water and electrode polarization with backfilling of the pore space with excess free water. Monitoring the transient amplitude directly, we follow variations in reaction rate with changes in temperature and addition of chemical retarders. We compare reaction rates with other measures of hydration, such as heat evolution by isothermal calorimetry, bound-water formation by thermogravimetric analysis, and calcium hydroxide production by differential scanning calorimetry. We monitor backfilling of the pore space with excess water over long periods of time and monitor the cure of precast concrete obtained from production runs.

Future work will explore a variety of signal changes occurring in each component with material and processing changes through a combination of analytical measurement, chemical variation, and experimental investigation.

Acknowledgements

The authors would like to acknowledge Mr. Geoffrey Betz of Elizabethtown College, who performed the DSC measurements in this work.

References

[1] Neville, A. M., 1996, Properties of Concrete, Fourth Edition, John Wiley and Sons, New York, NY, pp. 25-37.

[2] Karl J. Bois, Aaron D. Benally, Paul S. Nowak, Reza Zhoughi, *IEEE Trans Instrum. and Msmt.*, Vol 47, No 3, June 1998.

[3] A van Beek, Dielectric Properties of Young Concrete, PhD Thesis, (Delft Univ. Netherlands, 2000).

[4] Beek A. van, Lokhorst S.J., van Breugel K., On-site determination of hydration and associated properties of hardening concrete, Nondestructive Evaluation of Civil Structures and Materials, Boulder, CO, pp. 349-363, 1996

[5] N. E. Hager III and R. C. Domszy, *J. Appl. Phys.* 96, 5117-5128 (2004).

[6] R. H. Cole, J. G. Berberian, S. Mashimo, G. Chryssikos, A. Burns, and E. Tombari, *J. Appl. Phys.* 66, 793 (1989).

[7] N.E. Hager III, *Rev. Sci. Instrum*. 65 (4), 887 (1994).

[8] D. P. Bentz, X. Feng, C. J. Haecker, and P. E. Stutzman, "Analysis of CCRL Proficiency Cements 135 and 136 Using CEMHYD3D", NIST Internal Report 6545 (NIST, Gaithersburg, Md. August 2000).

[9] D. P. Bentz, C. J. Haecker, X. P. Feng and P. E. Stutzman, "Prediction of Cement Physical Properties by Virtual Testing," Process Technology of Cement Manufacturing. Fifth International VDZ Congress. Proceedings, (Düsseldorf, Germany, September 23-27, 2002) pp. 53-63.

[10] W. J. McCarter, T. M. Chrisp, and G. Starrs, *Cement and Concrete Research,* 33 (2), 197-206 (2003).

[11] W. J. McCarter, T. M. Chrisp, and G. Starrs, *Cement and Concrete Composites* 21, 277-283 (1999).

[12] Nobuhiro Miura, Nobuyuki Asaka, Naoki Shinyashiki, and Satoru Mashimo, *Biopolymers*, 34, 357-364 (1994).

[13] Nobuhiro Miura, Yoshihito Hayashi, Naoki Shinyashiki, and Satoru Mashimo, *Biopolymers*, 36, 9-16 (1995).

[14] Tomoyuki Ishida, Tomoyuki Makino, and Changjun Wang, *Clay and Clay Minerals* 48 (1), 75 (2000).

[15] E.J. Garboczi and D.P. Bentz, *J. Mater. Sci*. 27, 2083-92 (1992).